Towards *In Situ* X-Ray Diffraction Imaging at the Nanometer Scale: Early Detection of Nanoparticle Growth in Light Metal Alloys

X-ray diffractive imaging is widely used for nondestructive, high-resolution bulk-material characterization. Coherent X-ray imaging, though very powerful, has stringent requirements on the spatial isolation of a small sample, optics stability and X-ray coherence, while suffering from limitations in detector pixel resolution and insufficient dynamical range. Transmission electron microscopy offers very high resolution, but sample preparation is destructive and multiple scattering limits the technique to surface studies or very thin samples (<0.5 μm).

Novel materials with properties governed by the dispersion of nanoparticles embedded *within* a continuous bulk matrix (such as technologically important light metal alloys) thus require a complementary technique that can offer nondestructive 3D characterization of the nanoparticle form and dimensions by averaging over a substantial volume of nanoprecipitates, rather than a single isolated particle. We have developed an innovative X-ray diffraction technique aimed specifically at characterizing such materials at the nanometer scale. Established on various embedded nanoparticles [1], we are extending the technique to potential real time *in situ* investigations. Due to the complexity of nucleation and growth kinetics of the nanoprecipitates, it is crucial for such *in situ* studies to be sensitive to the early stages of precipitate formation.

Principal experiments were performed on the high-resolution multi-axis diffractometer at beamline **BL13XU**. The nondispersive triple axis setup is shown in Fig. 1. The arrangement consisted of a double-reflection, channel-cut Si(400) monochromator (axis 1), used to select 10.9 keV X-rays, with slits limiting the beam size to 0.25 mm vertically and 1.00 mm horizontally. The sample was placed downstream of the monochromator, resulting in a modulated wave incident on the single-reflection Si(400) analyzer crystal (mounted on the goniometer stage, axis 2). A scintillation counter was mounted on the 2θ-arm (axis 3). The sample was 0.6-mm-thick single-crystal Al-2.0%wt Cu, polished and chemically etched with $[100]_{Al}$ normal to the surface. Solutionizing (530 °C for 1 h), water quenching, and ageing at 150 °C for 172 h resulted in randomly distributed, weakly diffracting, Al_2Cu nanoprecipitates, crystallographically oriented along the $<100>_{Al}$ planes (Fig. 2).

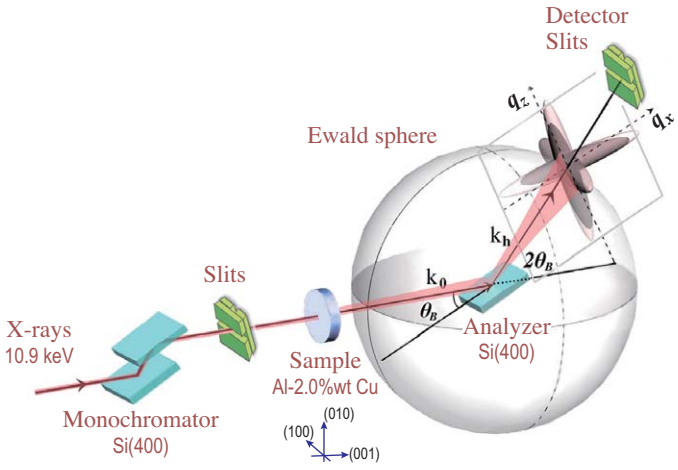

Fig. 1. Schematic of triple axis diffractometry setup.

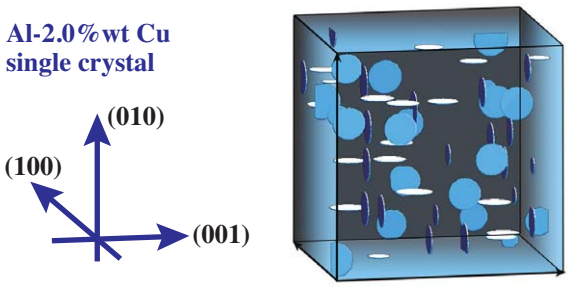

Fig. 2. Simulated volume of embedded nanoparticles, representative of the size spread of Al_2Cu nanoprecipitates in artificially aged Al-2.0%wt Cu.

We collected a 2D reciprocal space map (RSM) around the Si(400) Bragg reflection of the analyzer by performing α/2θ scans (along q_z in Fig. 1), with shifts of the analyzer, α, in between. Results from two sample orientations are shown in Figs. 3(c) and 3(d), and are compared with those of a plane wave incident on the analyzer (no sample) in Fig. 3(e). The results shown span an angular range of α = ±0.795°, and Δ2θ = ±1.590°, with nominal step sizes of 0.01° and 0.02°, respectively. Here, α and Δ2θ are deviations of the analyzer and detector-slit arrangement from their ideal Bragg configurations.

On a background of widespread diffuse scattering, there are dynamical and kinematical diffraction streaks. Along q_z is the crystal truncation rod, resulting from the abrupt change in electron density at the surface of the analyzer. The angular allowance of the detector slits (0.25 mm vertically and 5.0 mm horizontally) caused the thin, single-pixel,

detector streak at an angle of θ_B counterclockwise from the q_z axis, i.e., tangential to the Ewald sphere.

The diffracted wavefront emerging from the sample imitated the effect of mosaicity in the analyzer crystal, as evident in the horizontal streaks of Figs. 3(c) and 3(d), and simulated in 3(a). The shortened horizontal streak with more prominent asymmetry in Fig. 3(d) is due to a different projection (onto the Ewald sphere) of the 3D diffracted intensity of the sample, resulting from azimuthal sample rotation [1,4]. The simulated RSMs were calculated using Takagi equations [2] (Figs. 3(a) and 3(b)), assuming a weakly diffracting object, where the nanoprecipitates were approximated as flat cylinders with a Gaussian distribution of diameters (Fig. 1) [4].

By deconvolving the instrumental effects and applying a modified Fienup Gerchberg Saxton error-reduction algorithm [1,3,4], we reconstructed a pseudo-3D image using *a priori* knowledge about the symmetry of the nanoprecipitates. The reconstruction of a single Al_2Cu nanoprecipitate, in Figs. 3(g) and 3(h), is representative of the modal (most commonly occurring) nanoprecipitate size. A transmission electron micrograph of two randomly chosen nanoprecipitates is shown in Fig. 3(f).

In the present work, the sensitivity of the technique to the presence and crystallographic orientation of sparse, weakly diffracting embedded nanoprecipitates, was established. Not only is this a fundamental step in the characterization of static intermetallic nanostructures in bulk alloys, but it warrants the extension of the technique to real time *in situ* investigations. The first successful *in situ* experiments, in which the nucleation, clustering and very early stages of nanoprecipitate growth were examined have already been conducted at BL13XU [5]. The continuation of this work is now in progress.

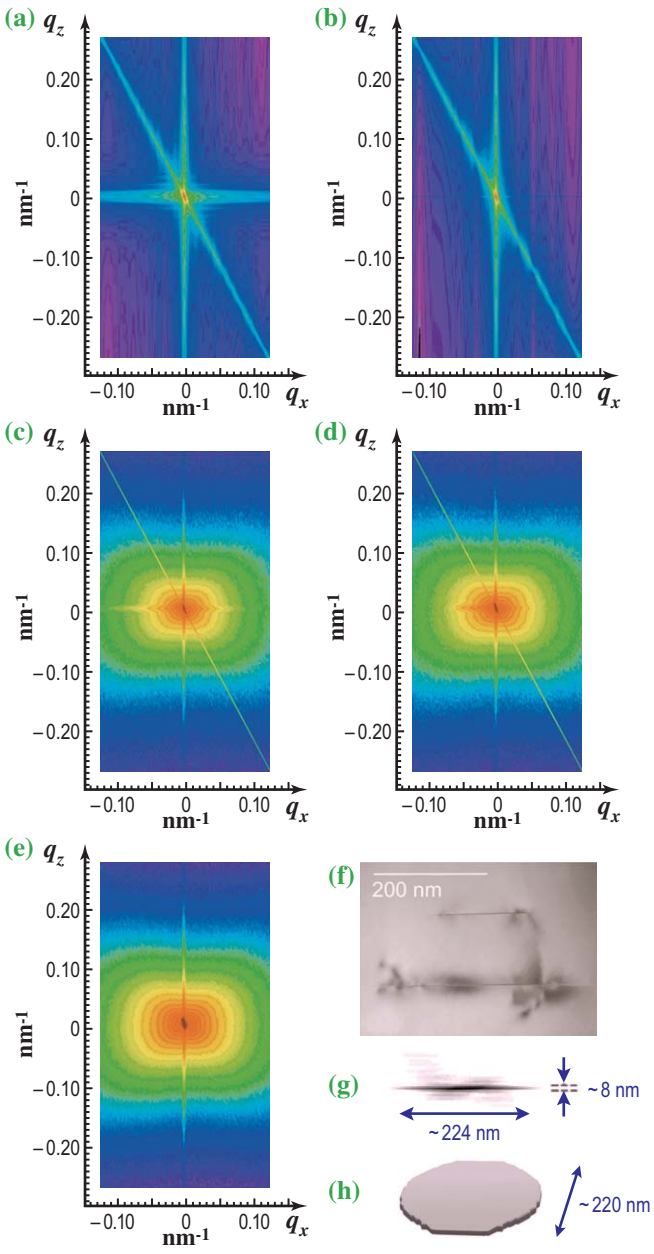

Fig. 3. Reciprocal space maps around the Si(400) analyzer reflection. Simulations: **(a)** Al-2.0%wt Cu single crystal, showing prominent horizontal streak; **(b)** no sample; Experimental results: **(c)** Al-2.0%wt Cu single crystal with nanoprecipitates parallel and perpendicular to diffracting plane; **(d)** nanoprecipitates at ±45° to diffracting plane; (e) no sample; **(f)** $<100>_a$ zone axis TEM micrograph showing 2 typical nanoprecipitates; Reconstructions: **(g)** 2D projected thickness of the modal nanoparticle (one variant shown); **(h)** pseudo-3D rendering of nanoparticle based on **(g)**.

N. A. Zatsepin[a], A. Y. Nikulin[a,*], R. A. Dilanian[a] and O. Sakata[b]

[a] School of Physics, Monash University, Australia
[b] SPring-8/JASRI

*E-mail: andrei.nikulin@sci.monash.edu.au

References

[1] A. Y. Nikulin *et al.*: Nano Letters **7** (2007) 1246.
[2] S. Takagi: Acta Cryst. **15** (1962) 1311.
[3] J.R. Fienup: Appl. Opt. **21** (1982) 2758.
[4] *N.A. Zatsepin, R.A. Dilanian, A.Y. Nikulin, B.M. Gable, B.C. Muddle and O. Sakata: Appl. Phys. Lett.* ***92*** *(2008) 134101.*
[5] N.A. Zatsepin *et al.*: submitted.